

Casing Collar Identification using AlexNet-based Neural Networks for Depth Measurement in Oil and Gas Wells

Siyu Xiao[✉], Xindi Zhao[✉], Tianhao Mao[✉], Yiwei Wang[✉], Yuqiao Chen[✉],
Hongyun Zhang[✉], Jian Wang[✉], Junjie Wang[✉], Shuang Liu[✉], Tupei Chen[✉] and Yang Liu^{✉*}

Abstract—Accurate downhole depth measurement is essential for oil and gas well operations, directly influencing reservoir contact, production efficiency, and operational safety. Collar correlation using a casing collar locator (CCL) is fundamental for precise depth calibration. While neural network-based CCL signal recognition has achieved significant progress in collar identification, preprocessing methods for such applications remain underdeveloped. Moreover, the limited availability of real well data poses substantial challenges for training neural network models that require extensive datasets. This paper presents a system integrated into downhole tools for CCL signal acquisition to facilitate dataset construction. We propose comprehensive preprocessing methods for data augmentation and evaluate their effectiveness using our AlexNet-based neural network models. Through systematic experimentation across various configuration combinations, we analyze the contribution of each augmentation method. Results demonstrate that standardization, label distribution smoothing (LDS), and random cropping are fundamental requirements for model training, while label smoothing regularization (LSR), time scaling, and multiple sampling significantly enhance model generalization capability. The F1 scores of our two benchmark models trained with the proposed augmentation methods maximumly improve from 0.937 and 0.952 to 1.0 and 1.0, respectively. Performance validation on real CCL waveforms confirms the effectiveness and practical applicability of our approach. This work addresses the gaps in data augmentation methodologies for training casing collar recognition models in CCL data-limited environments.

Index Terms—Casing collar locator, Depth Measurement, Downhole Positioning, Neural Network, Pattern Recognition

I. INTRODUCTION

ACCURATELY positioning downhole tools – including perforating guns, bridge plugs, and packers – relative to target zones is essential in modern oil and gas well operations, directly affecting reservoir contact,

Siyu Xiao, Tianhao Mao, Yiwei Wang, Yuqiao Chen, Junjie Wang, Shuang Liu and Yang Liu are with the State Key Laboratory of Thin Solid Films and Integrated Devices, University of Electronic Science and Technology of China, Chengdu 611731, China.

Xindi Zhao, Hongyun Zhang and Jian Wang are with the Southwest Branch of China National Petroleum Corporation Logging Co., Ltd., Chongqing 401100, China.

Tupei Chen is with Nanyang Technological University, Singapore 639798.

*Corresponding author.

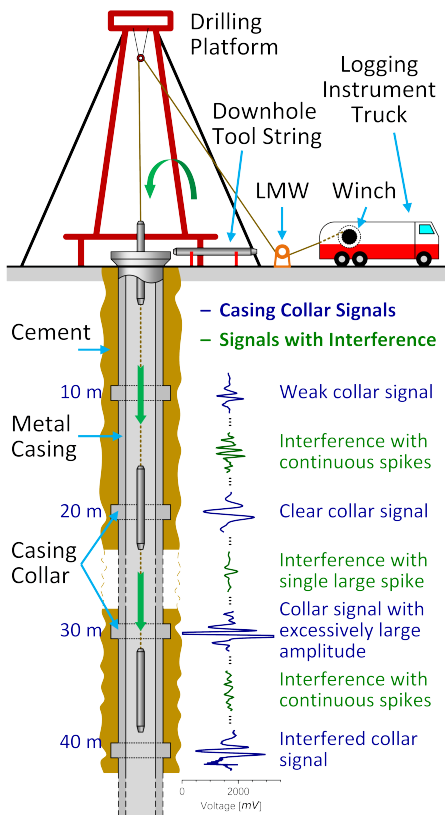


Fig. 1. Cross-sectional illustration of a typical oil and gas well structure. Representative casing collar signals from magnetic response are illustrated in dark blue near the corresponding casing collar, while the typical interference signals distant from casing collars are illustrated in dark green. Refer to figures from [1].

production efficiency, and operational safety [2]. Central to this task is precise downhole depth measurement, a challenge compounded by the extreme geometries of wellbores, as shown in Fig. 1 organized from [1], which often span thousands of meters in length while maintaining diameters of only a few inches [3].

Although a length measuring wheel (LMW) is able to estimate depth as tools descend during wireline intervention operations, its accuracy remains insufficient. To improve depth measurement accuracy, calibration using signals from a casing collar locator (CCL) – a magnetic downhole positioning tool that detects magnetic

anomalies at the casing collars of wellbores or pipes – is fundamental [4]. The CCL produces a characteristic magnetic response as an electrical signal when passing through each collar, termed a “collar signal” or “collar magnetic signature”. The characteristic magnetic response pattern typically exhibits a bimodal distribution, as illustrated by dark blue waveforms in Fig. 1. Through collar correlation, which refers to matching CCL logs with casing tally, depth reference markers are established, enabling actual and accurate depth measurement [5], [6]. The casing tally, also known as the list of collars or casing string reference depths, records the depths of casing collars and is commonly extracted from cementing quality data.

While collar correlation using CCL signals is an established method, collar signal recognition presents significant challenges. CCL signal integrity can be severely compromised by multiple factors, including cable effects, wellbore conditions [7], tool motion (swing or rotation), amplifier saturation, and environmental noise [5], [8]. Consequently, collar signal waveforms become increasingly ambiguous, necessitating robust recognition of collar signals amid various interferences, as illustrated by dark green waveforms in Fig. 1.

Various signal processing techniques have been developed to identify collar signals under interference conditions. Traditional methods include fixed or dynamic thresholding [1], [9], digital filters and template-based cross-correlation [10], time-frequency domain techniques such as Fourier or wavelet transforms [11], and physical plausibility filters [1], [4], [12]. However, these approaches exhibit limited generalizability [8], [12]. With the emergence of machine learning, researchers have increasingly employed deep neural networks to automate collar signal recognition. These developments include convolutional neural networks (CNNs) and long short-term memory networks (LSTMs) [13]–[15]. Additionally, advanced architectures such as transformer models [16] and physics-informed neural networks (PINNs) [17] have been proposed for downhole signal classification, anomaly detection, and denoising tasks [18].

Nevertheless, significant challenges persist. Neural networks require substantial volumes of labeled training data, which are often unavailable or difficult to obtain in downhole environments [13], [19]. This scarcity means that the available data for training collar recognition neural networks are considerably less than those for other tasks such as face recognition or image classification. Therefore, efficiently utilization of existing data is indispensable.

The limited sample amount and unique characteristics of CCL signal data necessitate specialized preprocessing methods for neural network training. However, research on preprocessing methods remain scarce, despite exten-

sive work on collar signal recognition [4], [8], [10]–[13], [16]–[18]. Fortunately, extensive work exists on data augmentation for preventing overfitting and improving generalizability when training on small datasets. Data normalization methods – including min-max scaling, Z-score normalization (standardization), and robust scaling – demonstrate important roles in stabilizing input distributions and gradients, preventing vanishing and exploding gradients, and ultimately accelerating training convergence [20]–[23]. Label smoothing regularization (LSR) and label distribution smoothing (LDS) discourage overconfident predictions, thereby enhancing model generalizability [24], [25]. Similarly, employing probability maps for boundary prediction instead of one-hot encoding (OHE) labels through boundary probabilization transforms the training objective from single-point prediction to probability distribution estimation, enabling models learn smooth and fuzzy decision boundaries that are more resistant to noise or perturbations [14], [24], [26]. Notably, Gaussian kernel often deliver optimal results in LDS applications [24]. Furthermore, graph augmentation techniques including randomly cropping, scaling, translation, and noise injection expand training datasets while improving model generalizability and robustness [27], [28].

The main contributions of this paper are as follows:

- We develop a system integrated into downhole tools, called the Signal Collecting Vessel (SCV), illustrated in Fig. 2. The SCV samples original CCL signal within wellbores or pipes, converts them to digital format, and stores them as waveforms for dataset construction.
- We propose two neural networks models for collar signal recognition that serve as benchmarks for evaluating data preprocessing methods, as illustrated in Fig. 3. The first model, Thin AlexNet (TAN), is modified from AlexNet – a classic and proven architecture in pattern recognition. The second model, Miniaturized AlexNet (MAN), is a simplified version of TAN with fewer layers.
- We propose several data augmentation methods for preprocessing original waveforms to enhance model training performance, including normalization, label distribution smoothing (LDS), label smoothing regularization (LSR), time scaling, cropping and translation, amplitude jittering, noise injection, and multiple sampling.
- We conduct extensive experiments across various configuration combinations to validate our methods. Results demonstrate that standardization, LDS, and random cropping are fundamental requirements for models training, while LSR, time scaling, and multiple sampling significantly enhance model generalization capability.

II. METHODS

A. Problem Transformation

As previously discussed, accurately positioning downhole tools through collar correlation relies on correct identification of bimodal patterns (i.e., collar signals) within CCL signals. The center of each bimodal pattern is typically considered as the moment when the CCL coincides with the casing collar.

By observing signal characteristics, collar signals can be clearly identified from signals proximate to the corresponding collar rather than from distant signals. Therefore, collar signal identification is largely independent of CCL signals on large time scales. Consequently, focusing on CCL signal fragments using an appropriately sized sliding window is reasonable, consistent with approaches in [14] and [15]. When CCL signals are sampled at a fixed frequency, the absolute value of timestamps within sliding windows becomes irrelevant, indicating that the pure CCL signal sequence sufficiently conveys the necessary information.

As shown in Fig. 1, the casing tally indicates a series of depths that can be mapped to collar signals on the signal timeline as a series of marks. The center points of collar signals marked on the timeline (hereafter referred to as “collar marks”) constitute a series of timestamps that require different representation when captured by sliding windows. The most direct method for representing collar marks is one-hot encoding (OHE), where 1 denotes “is a collar mark” and 0 denotes “is not a collar mark”. This approach transforms collar mark prediction into a binary classification problem.

However, collar marks exhibit extreme sparsity. Consequently, the number of 0s exceeds that of 1s by several orders of magnitude, representing severe class imbalance. Due to the nature of backpropagation neural networks (BPNNs), gradients become spare and penalties are unevenly distributed, causing training instability and slow convergence. This ultimately renders effective classifier training nearly impossible. To address this issue, one-hot encoding is replaced with a probability map [14], [29], where labels represent the probability of boundary occurrence. Interestingly, according to the theory in [29], label represents the distribution of relative importance across possible categories (i.e., “is a collar mark”). This replacement transforms boundary classification into boundary membership classification, providing meaningful feedback during backpropagation and ultimately enabling stable and efficient network training.

B. Collecting the original CCL waveforms

As shown in Fig. 2, the Signal Collection Vehicle (SCV) is designed for integrating into downhole tools. The SCV comprises several submodules, including the

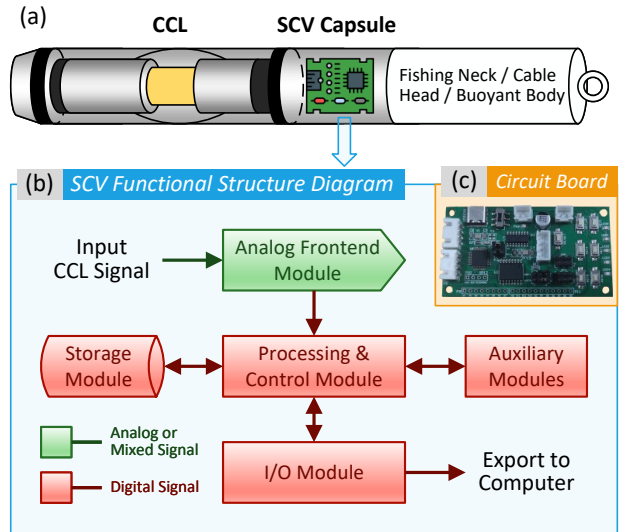


Fig. 2. Structure of downhole tools integrated with the Signal Collection Vehicle (SCV): (a) Schematic diagram of the internal structure of the perforating gun employed in this work; (b) Functional structure diagram of the SCV; (c) A SCV circuit board.

analog frontend (AFE) module, the signal processing and control module, the data storage module, the input-output (I/O) module, and auxiliary modules. Once the SCV begins operation, the AFE module samples CCL signals at 1 kHz via an analog-to-digital converter (ADC), converting them to digital format, and the control module stores these digital data in the storage module. Following completion of downhole operations, the SCV is salvaged to export data via the I/O module.

By sampling CCL signals downhole and eliminating long cable transmissions, signal integrity is preserved. The signals sampled by the SCV are designated as “original CCL waveforms” and form the foundation for dataset construction, as illustrated in Fig. 3(a).

C. Dataset and Augmentation

Based on the original CCL waveforms, collar marks are manually annotated through expert analysis. For model training, CCL waveforms and their corresponding labels (in one-hot encoding) are segmented, with each segment containing a collar mark at its center, as illustrated in Fig. 3(a). Portions distant from collar marks are excluded.

To enhance training effectiveness and maximize data utilization, we present various data augmentation methods for preprocessing original CCL data. These methods encompass data normalization, regularization, transformation and multiple sampling, which can be applied independently or in combination, as illustrated in Fig. 3(b).

After preprocessing, the augmented segments and labels constitute the datasets used for model training and evaluation.

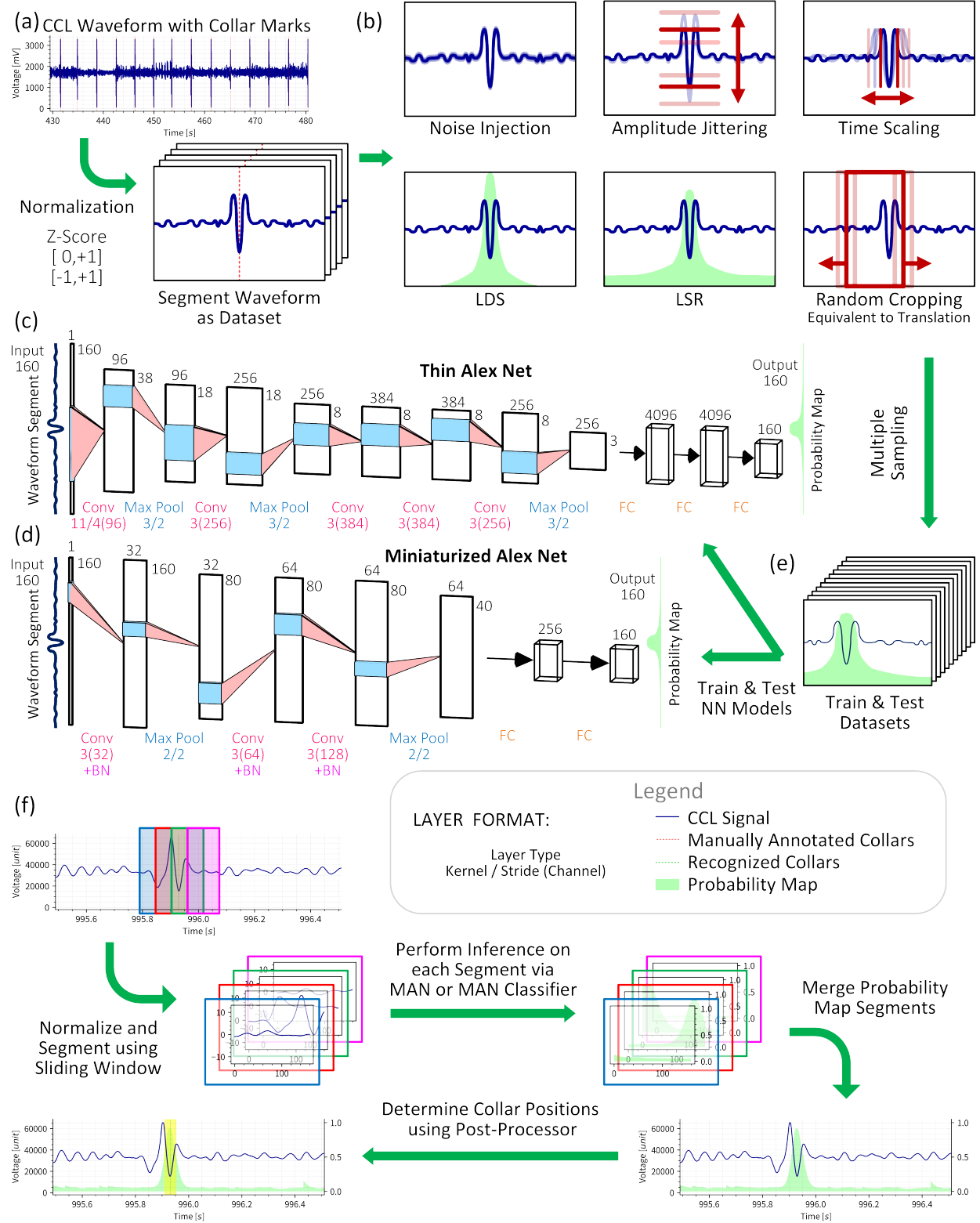


Fig. 3. The train and inference process of this work: (a) Segment normalized CCL waveform with manually labeled collar marks, each segment containing a collar mark at its center (signal shapes in boxes are illustrative only); (b) Augmentation methods for preprocessing waveform segments; (c)-(d) Neural network architectures employed in this work; (e) Multiple random augmentations applied to each segment generate diverse sub-segment variants for training and testing datasets; (f) The procedure of casing collar recognition from CCL waveforms using sliding windows with overlap.

1) Normalization of waveforms:

The original CCL waveform represents raw data from the ADC in unsigned integer format. Theoretically, raw data requires normalization to enhance training performance, particularly convergence speed [30]. Both min-max scaling and z-score normalization warrant investigation. For min-max scaling, waveforms are transformed to either $[0, 1]$ or $[-1, 1]$. The minimum and maximum values derive from either the waveform's dynamic range or the ADC specifications.

2) Label Distribution Smoothing (LDS):

Convolving a kernel with the empirical density distribution produces a kernel-smoothed version. The effective label density distribution is defined as [24]:

$$p'(y') \triangleq \int_{\mathcal{Y}} k(y, y') p(y) dy \quad (1)$$

where $p(y)$ is the label of y in the training data; p' is the effective density of label y' ; and $k(y, y')$ is the kernel function.

One-hot encoding of collars along the timeline constitutes a validity probability distribution that proves challenging for training. Convolution smooths these hard labels, enabling each label in the validity probability distribution to incorporate information from neighboring labels [24].

While Gaussian kernels reportedly achieve optimal results among all kernel types [24], other research cautions that Gaussian assumptions may not accommodate complex real-world datasets [29]. This work employs a Gaussian kernel is employed, yielding the following label formulation:

$$p'(t) = \begin{cases} \sum_i \sum_t e^{-\frac{(t-t_i)^2}{2\sigma^2}} & , \quad if < 1 \\ 1 & , \quad otherwise \end{cases} \quad (2)$$

where σ is the Gaussian root mean square (RMS) width; t_i is the moment when the i^{th} collar occurs.

3) Label Smoothing Regularization (LSR):

LSR softens labels by redistributing a small probability portion from the correct class evenly among all classes. The distribution relationship follows [25]:

$$\begin{aligned} p(k) &= \delta_{k,i} \\ p'(k) &= (1 - \epsilon) \delta_{k,i} + \frac{\epsilon}{K} \\ \delta_{k,i} &= \begin{cases} 1 & , \quad k = i \\ 0 & , \quad k \neq i \end{cases} \end{aligned} \quad (3)$$

where $p(k)$ is the ground-truth distribution over the k^{th} class; $p'(k)$ is the training distribution over the k^{th} class; i denotes the correct class; K is the total number of classes; and δ is the Kronecker delta function.

This method discourages overconfident predictions by preventing the largest logit from becoming disproportionately larger than others, thereby regularizing the model and enhancing its generalization capability [25]. For this work, with $K = 2$, the training distribution simplifies to:

$$p'(k) = (1 - \epsilon)p(k) + \frac{\epsilon}{2} \quad (4)$$

4) Geometric Transformations:

The dataset undergoes expansion through various geometric transformations, as illustrated in Fig. 3(b). The following transformations are employed:

- **Time Scaling:** Original sub-segments are scaled along the time axis by random factors and subsequently resampled to match the ADC sampling rate. To compensate for frequency distortion introduced by resampling, the Whittaker-Shannon interpolation formula (i.e., sinc interpolation) is chosen.
- **Randomly Cropping and Translation:** These transformations segment waveforms into sub-segments that match both the sliding window length and the neural network model's input length.
- **Amplitude Jittering:** Original sub-segments are multiplied by random gain factors to enhance the model's robustness and generalization capability.
- **Noise Injection:** Gaussian noise is added to original sub-segments to improve model robustness against noise.
- **Flipping:** Voltage or time axis flipping is excluded as such transformations would violate the physical principles governing CCL magnetic response.

5) Multiple Sampling:

To maximize dataset utilization, each segment undergoes multiple random augmentations to generate diverse sub-segment variants, as illustrated in Fig. 3(e). This approach theoretically accelerates convergence and enhance augmentation effectiveness.

D. Neural Network

The proposed model, Thin AlexNet (TAN), is a time-series version of the classical AlexNet architecture. The input and output dimensions are reduced from 2D to 1D to adapt CCL signals. Since AlexNet has demonstrated success in image classification [27], [28] and possesses sufficient simplicity to clearly demonstrate the effects of data augmentation, the TAN model serves as an appropriate benchmark.

The TAN model comprises 5 convolutional layers with ReLU activation, 3 max pooling layers, and 3 fully connected (FC) layers, with ReLU activation applied to the first two fully connected layers, as illustrated in Fig. 3(c). The input of model is a fixed-length segment from a waveform. And the output produces a series of logits representing scores of collar mark classification for

each temporal position within the input segments. This differs from the original AlexNet. Probability for each temporal position is obtained through sigmoid function.

Based on TAN model, we proposed a simplified version, Miniaturized AlexNet (MAN), as illustrated in Fig. 3(d). MAN contains fewer convolutional layers, max pooling layers and fully connected layers than TAN. Additionally, batch normalization (BN) layers are appended in MAN to improve training stability. MAN employs the same input-output format as TAN.

III. EXPERIMENTS AND RESULTS

A. Evaluation Measures

To evaluate the classifiers implemented by TAN and MAN, which output probability distributions for classification, metrics that measure distance and similarity between predicted and label distributions are appropriate [29]. F1 score and cross-entropy (CE) represent standard choices for such evaluation. Additionally, the area under the precision-recall curve (AUC-PR) provides objective performance assessment for binary classifiers.

To recognize collar signals from normalized long CCL waveforms, a sliding window of width W with a stride of $\lfloor W/2 \rfloor$ is employed. This configuration produces 50% overlap between consecutive windows, ensuring that each overlapping region is captured by exactly two adjacent windows. The window advances through the waveform in half-width increments, balancing computational efficiency with temporal resolution while maintaining analytical continuity. The probability map segments inferred from overlapping regions of adjacent windows are averaged to produce the complete probability map, as illustrated in Fig. 3(f).

Through sliding window progression, the complete probability map for the entire CCL waveform is generated. Continuous intervals with probabilities exceeding the threshold are identified as valid regions, with their center positions designated as collar marks. This procedure constitutes the “post-processing” stage. The complete casing collar recognition process from waveform comprises a neural network-based classifier and a post-processor for probability map analysis, as illustrated in Fig. 3(f). Collar recognition performance is evaluated by comparing recognized collar positions with manually annotated reference positions. Recognized collars within the neighborhood of annotated collars are classified as true positives, while those elsewhere are classified as false positives. Missed collars are considered as false negatives. Precision, recall and F1 score are calculated for evaluation.

The CCL waveforms used in experiments originate from actual oil wells in Sichuan Province, China, ensuring that results are objective and representative of real-world conditions.

B. Training and Testing

The training set comprises three-quarters of the CCL signal waveforms, with the remaining quarter allocated to the test set. The models are trained with a batch size of 16 for 100 epochs utilizing cross-entropy loss (CE loss) with an adaptive moment estimation (Adam) optimizer, implemented in PyTorch. Key configurations (Cfgs.) are presented in Tables I and II. The training progress and the optimal model performance for each configuration are illustrated in Fig. 4. Additionally, a mild interference waveform and a moderate interference waveform are evaluated through model inference, post-processing, and statistical collar identification performance analysis. The results for precision, recall, and F1 score are tabulated in Tables I and II.

C. Results and Analysis

To explore the validity and importance of augmentation methods, several real and complete waveforms are experimented to verify the models’ ability of predicting collar positions. The experimental results are indexed and divided into 3 groups, as illustrated in Fig. 4, with curve indexes corresponding to those in Tables I and II. The first group (Cfgs. 1-6) examines normalization methods, label distribution methods, and cropping methods. The second group (Cfgs. 7-12) investigates label smoothing, noise injection, amplitude jittering, and time scaling. The final group (Cfgs. 13-18) explores optimal combination configurations.

1) Fundamental Preprocessing Requirements:

Comparison of Cfgs. 1 and 3, which differ in label distribution method, confirms that F1 score for both classifier and recognition using one-hot encoding approaches 0, despite the CE loss decreasing more rapidly than with LDS. The probability maps corroborate this observation, as illustrated in Figs. 5(a,c). This indicates that one-hot encoded collar labels are difficult for models to learn, as the loss function reaches a local minimum when models consistently output negative predictions, as illustrated in Fig. 4(a).

Similar phenomena occur with min-max normalization versus standardization (corresponding to Cfgs. 3-5), and fixed cropping versus random cropping (corresponding to Cfgs. 2 and 3), as illustrated in Figs. 5(b,c). Waveforms processed with min-max normalization prove challenging for model training. Furthermore, models using fixed cropping learn only sliding window positions rather than waveform characteristics.

Comparison of Cfgs. 3 and 6 clearly demonstrates that both TAN and MAN module have the ability to estimate collar positions when using LDS, standardization, and random cropping, as illustrated in Figs. 5(c,d). However, MAN training proceeds more slowly than TAN training,

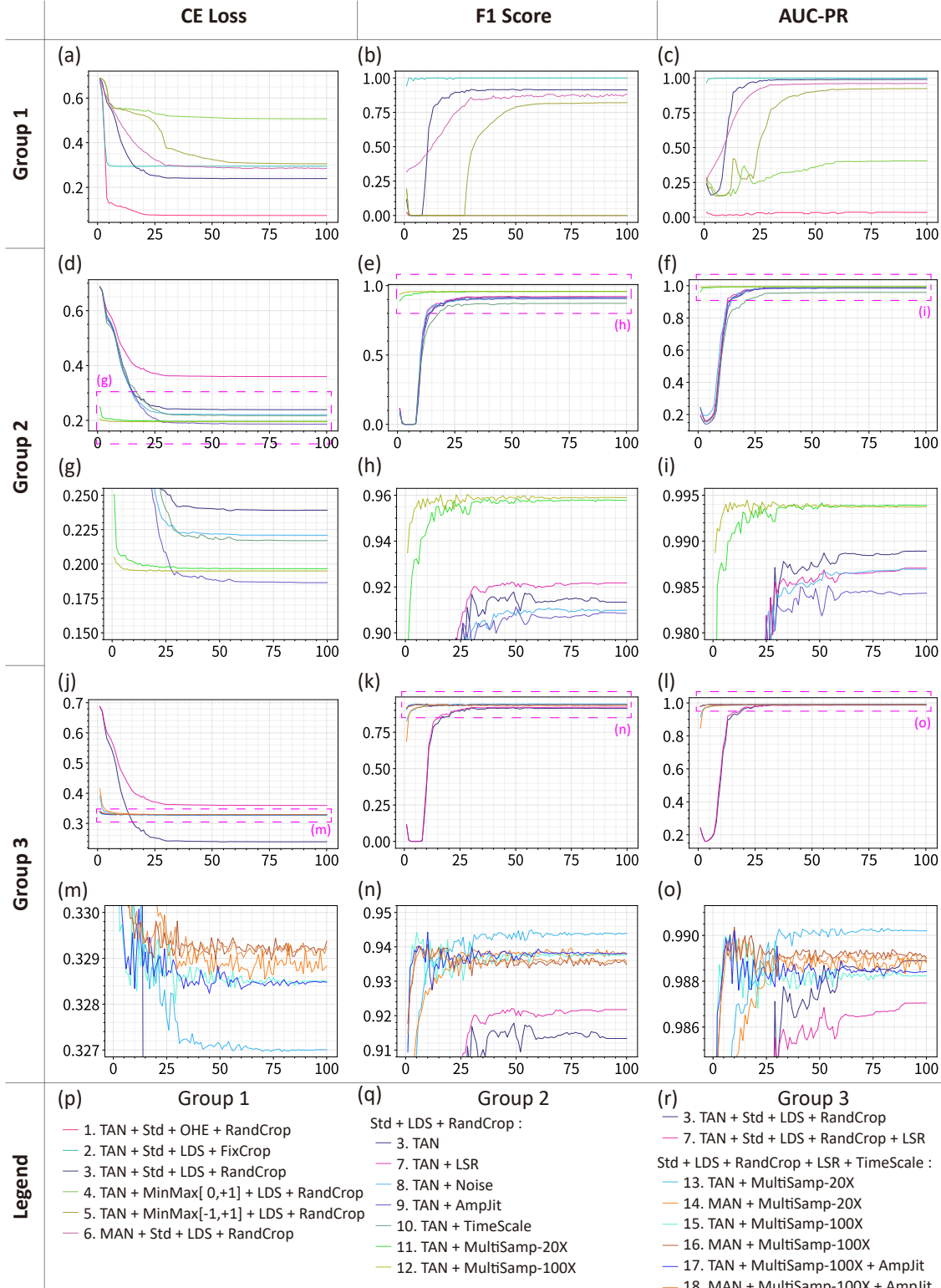


Fig. 4. Evaluation metrics of training progress under different configurations, including cross-entropy loss, F1 score, and area under the precision-recall curve (AUC-PR). The curve indexes correspond to configurations in Tables I and II. The meanings of abbreviations refer to Tables I and II. (a)-(c) Evaluation metrics for Group 1 configurations; (d)-(f) Evaluation metrics for Group 2 configurations; (g)-(i) Enlarged sections of (d)-(f); (j)-(l) Evaluation metrics for Group 3 configurations; (m)-(o) Enlarged sections of (j)-(l); (p)-(r) legends for (a)-(c), (d)-(i), and (j)-(o), respectively.

TABLE I
EXPERIMENTAL RESULTS FOR VARIOUS COMBINATIONS OF NORMALIZATION, LABEL DISTRIBUTION, AND CROPPING METHODS

Cfg. No.	Model	Normalization	Lbl. Dis.	Crop	Evaluation by Validation Set during Train			Evaluation by Moderate Interference Waveform			Evaluation by Mild Interference Waveform		
					CE	F1	AUC-PR	P	R	F1	P	R	F1
1	TAN	Standardization	OHE	Rand	0.0736	0	0.0350	0	0	0	0	0	0
2	TAN	Standardization	LDS	Fix	0.2943	1	0.9987	0	0	0	0	0	0
3	TAN	Standardization	LDS	Rand	0.2391	0.9134	0.9889	0.9136	0.9610	0.9367	0.9811	1	0.9905
4	TAN	MinMax [0,+1]	LDS	Rand	0.5074	0	0.4051	0	0	0	0	0	0
5	TAN	MinMax [-1,+1]	LDS	Rand	0.3055	0.8205	0.9234	0.0396	0.1169	0.0592	0.0335	0.1346	0.0536
6	MAN	Standardization	LDS	Rand	0.2852	0.8821	0.9619	1	0.9091	0.9524	1	1	1

All configurations use a batch size of 16, with no additional data augmentation methods applied.

Abbreviations: Cfg. No. = configuration number; Lbl. Dis. = label distribution; CE = cross-entropy; F1 = F1 Score; AUC-PR = area under the precision-recall curve; P = precision; R = recall; OHE = one-hot encoding; LDS = label distribution smoothing; Rand = random.

Configuration numbers are color-coded to match the corresponding curves in Fig. 4.

TABLE II
EXPERIMENTAL RESULTS FOR VARIOUS COMBINATIONS OF SOFT LABEL, GEOMETRIC TRANSFORMATIONS, AND MULTIPLE SAMPLING METHODS

Cfg. No.	Model	Soft Label	Noise Inj.	Amp. Jit.	Time Scale	Multi. Samp.	Evaluation by Validation Set during Train			Evaluation by Moderate Interference Waveform			Evaluation by Mild Interference Waveform		
							CE	F1	AUC-PR	P	R	F1	P	R	F1
3	TAN	-	-	-	-	1	0.2391	0.9134	0.9889	0.9136	0.9610	0.9367	0.9811	1	0.9905
6	MAN	-	-	-	-	1	0.2852	0.8821	0.9619	1	0.9091	0.9524	1	1	1
7	TAN	LSR	-	-	-	1	0.3596	0.9217	0.9871	0.9610	0.9610	0.9610	0.9811	1	0.9905
8	TAN	-	+	-	-	1	0.2209	0.9098	0.9869	0.8152	0.9740	0.8876	0.9630	1	0.9811
9	TAN	-	-	+	-	1	0.1864	0.9085	0.9843	0.9367	0.9610	0.9487	0.9811	1	0.9905
10	TAN	-	-	-	+	1	0.2170	0.8726	0.9592	0.9740	0.9740	0.9740	1	1	1
11	TAN	-	-	-	-	20	0.1966	0.9577	0.9939	0.9390	1	0.9686	1	1	1
12	TAN	-	-	-	-	100	0.1949	0.9589	0.9937	0.9872	1	0.9935	1	1	1
13	TAN	LSR	-	-	-	20	0.3270	0.9439	0.9902	0.9506	1	0.9747	1	1	1
14	MAN	LSR	-	-	-	20	0.3288	0.9379	0.9888	1	1	1	0.9811	1	0.9905
15	TAN	LSR	-	-	-	100	0.3285	0.9377	0.9883	0.9625	1	0.9809	1	1	1
16	MAN	LSR	-	-	-	100	0.3294	0.9348	0.9890	0.9744	0.9870	0.9806	0.9808	0.9808	0.9808
17	TAN	LSR	-	+	-	100	0.3285	0.9381	0.9884	0.9620	0.9870	0.9744	0.9811	1	0.9905
18	MAN	LSR	-	+	-	100	0.3293	0.9355	0.9889	0.9744	0.9870	0.9806	0.9808	0.9808	0.9808

All configurations employ standardization for normalization, LDS for label distribution, random cropping, and a batch size of 16.

Additional abbreviations: Inj. = injection; Amp. Jit. = amplitude jittering; Multi. Samp. = multiple sampling; LSR = label smoothing regularization.

with slightly inferior performance, as MAN contains approximately half the parameters of TAN. These findings establish that LDS, standardization, and random cropping are fundamental requirements for collar recognition model training.

2) Generalization Enhancement Methods:

To investigate the effects of LSR, noise injection,

amplitude jittering, and time scaling, Cfgs. 7-10 based on Cfg. 3 are experimented. Comparison of curves in Figs. 4(d-i) reveals that: (a) the final CE loss for Cfgs. 8-10 is lower than that for control Cfg. 3, while Cfg. 7 shows higher loss; (b) the classifier F1 scores of Cfgs. 7-9 are similar, while Cfg. 10 shows slightly lower performance; (c) LSR convergence is slower than others.

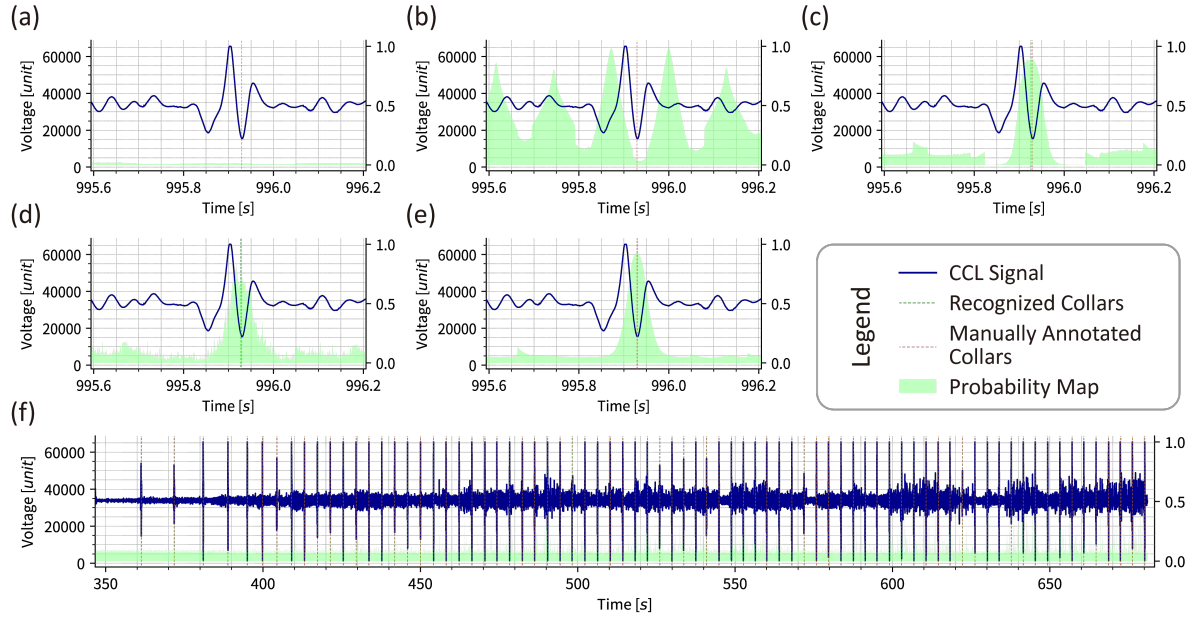


Fig. 5. Probability maps and recognition results for various configurations. (a) Cfg. 1 (using OHE); (b) Cfg. 2 (using fixed cropping); (c) Cfg. 3 (using LDS and random cropping); (d) Cfg. 6 (using fundamental methods with MAN model); (e) Cfg. 13 (optimal combination candidate using TAN model); (f) Full results of Cfg. 14 (optimal combination candidate using MAN model).

Performance comparison between Cfgs. 7-10 and control Cfg. 3, as tabled in Table II, demonstrates that: (a) LSR exhibits higher CE loss but superior F1 score in waveform evaluation, with 0.024 improvement on the moderate inference waveform; (b) although amplitude jittering and time scaling show lower F1 scores on validation set evaluation is compared to the control configuration, their waveform evaluation F1 scores are higher, with improvements of 0.012 and 0.037 respectively on the moderate inference waveform. These results suggest that LSR enhances generalization capability at the cost of convergence speed, while amplitude jittering and time scaling also improve generalization. However, noise injection performs worse than all other configurations. Additional experiments reveal that small noise provides limited benefits to performance, while large noise impairs performance. This likely occurs because real-world waveforms inherently contain small noise, and additional large noise hinders model learning waveform characteristics.

To investigate the effects of multiple sampling, Cfgs. 11-12 based on Cfg. 3 are experimented. Configurations with multiple sampling converge substantially faster than the control configuration, as shown in Figs. 4(d-i), because multiple sampling increases iterations per epoch. The F1 score improves up to 0.045 in evaluation. In summary, LSR, amplitude jittering, time scaling, and multiple sampling significantly enhance generalization capability, while noise injection provides limited benefits.

3) Optimal Configuration Identification:

Based on these conclusions, Cfgs. 13-18 are experimented to identify optimal combinations while comparing with Cfgs. 3, 6 and 7, as illustrated in Figs. 4(j-o) and 5(c-e) and tabulated in Table II. Several noteworthy phenomena emerge from these experiments.

First, metrics of configurations with 100x multiple sampling fluctuate more dramatically than those with 20x, suggesting the need for smaller initial learning rates when applying extensive multiple sampling. Second, simultaneous use of amplitude jittering and time scaling unexpectedly reduces the performance. We hypothesize that amplitude scaling compromises standardization benefits while improving generalization, as the relative amplitude of waveforms contains critical information. Third, Cfg. 13 achieves the highest CE loss and validation set F1 score among all TAN model configurations, yet its F1 score on the moderate interference waveform does not show corresponding improvement, as illustrated in Figs. 4(m-o). This occurs because multiple sampling introduces more randomly preprocessed samples, enhancing generalization capability.

Most significantly, MAN performance does not degrade substantially compared to TAN, and MAN exhibits less performance degradation on moderate interference waveform than TAN, despite containing approximately half the parameters, as tabulated in Table II. These findings suggest that: (a) TAN may experience overfitting in certain dimensions; (b) collar classification could

potentially be achieved with more compact networks warranting future investigation; (c) practical applications can consider the trade-off between accuracy and parameter count.

4) Performance Validation and Key Findings:

The results of Cfg. 14 are illustrated in Fig. 5(f) as an example, while the details of other experiments are not repeated here. Casing collars recognized by MAN model and collars labeled manually are marked in green and red, respectively. The casing collar positions are correctly recognized and align completely with manual annotations, providing the essential foundation for precise depth measurement.

These findings establish that the standardization, LDS, and random cropping are fundamental preprocessing requirements for collar recognition model training, while LSR, time scaling, and multiple sampling significantly enhance model generalization capability. The data augmentation methods achieve F1 score improvements of up to 0.063 for TAN model waveform evaluation and up to 0.048 for MAN model evaluation, compared to configurations using only fundamental methods, representing notable performance enhancements.

IV. CONCLUSIONS

This work developed the SCV to sample CCL signals downhole in the wellbore for datasets construction. We systematically analyzed the contributions of various data augmentation methods using benchmark evaluations on our proposed neural network recognition methodology. Experimental validation with authentic CCL waveforms confirm the effectiveness and validity of proposed approaches. This research addresses the existing gaps in data augmentation methodologies for training casing collar recognition models in CCL data-limited environments.

ACKNOWLEDGMENT

This work is supported by NSFC under project No. 62404033 and 62404034. This work is also supported by China National Petroleum Corporation Logging Co., Ltd. (CNLC) under project No. CNLC2023-7A01.

REFERENCES

- [1] S. Xiao, G. Ren, T. Mao, Y. Chen, Y. Liu, J. Wang, K. Tang, X. Zhao, Z. Yu, S. Liu, T. Chen, and L. Yang, “Realization of precise perforating using dynamic threshold and physical plausibility algorithm for self-locating perforating in oil and gas wells,” *arXiv preprint arXiv:2509.00608*, 2025.
- [2] M. H. Harris, “The effect of perforating oil well productivity,” *Journal of Petroleum Technology*, vol. 18, no. 04, pp. 518–528, 1966.
- [3] H. R. Seren and M. Deffenbaugh, “Miniaturized casing collar locator for small downhole robots,” *IEEE Sensors Letters*, vol. 6, no. 4, pp. 1–4, 2022.
- [4] J. O. Alvarez, E. Buzi, R. W. Adams, and M. Deffenbaugh, “Theory, design, realization, and field results of an inductive casing collar locator,” *IEEE Transactions on Instrumentation and Measurement*, vol. 67, no. 4, pp. 760–766, 2018.
- [5] R. Mijarez, D. Pascacio, R. Guevara, C. Tello, O. Pacheco, and J. Rodríguez, “Hptc cased-hole ccl tool enhancement via dsp techniques for accurate depth control in wire-line well interventions,” *Additional Papers and Presentations*, vol. 2014, no. HITEC, pp. 000 305–000 310, 2014.
- [6] H. Li, T. Tang, and Y. Wang, “Casing state detection methods based on the ccl signal of the tractor for horizontal wells,” in *2013 IEEE 11th International Conference on Electronic Measurement & Instruments*, vol. 2. IEEE, 2013, pp. 568–573.
- [7] J. Brown, “The effects of cable on signal quality,” *Sound and Video Contractor*, pp. 22–33, 1990.
- [8] H. Wang and W. Tang, “Application of computer automatic discriminating technology to the depth control of perforation,” *Well Logging Technology*, vol. 30, no. 4, p. 378, 2006.
- [9] H. Wang, H. Lv, J. Pan, G. Li, and X. Gao, “Study on collar depth identification based on relative amplitude method,” *J. Harbin Univ. Commer. (Nat. Sci. Ed.)*, vol. 28, no. 4, pp. 435–438, 2003.
- [10] J. Li, Y. Liu, J. Zhang, J. Wang, and Y. Zhang, “Application of cross-correlation function method in locating perforation depth,” *Journal of Southwest Petroleum University (Natural Science Edition)*, vol. 42, no. 6, pp. 42–48, 2020.
- [11] H. Li, J. Chen, Y. Xiao, X. Liu, and J. Wu, “Study on extracting traction device magnetic positioning information features based on anti-aliasing wavelet time entropy in the frequency domain,” *Chinese High Technology Letters*, vol. 20, no. 5, pp. 538–543, 2010.
- [12] Y. P. Yang, G. H. Luan, L. F. Zhang, M. Y. Niu, G. G. Zou, X. L. Zhang, J. Y. Wang, J. F. Yang, and M. S. Li, “Leak identification and positioning strategies for downhole tubing in gas wells,” *Processes*, vol. 13, no. 6, p. 1708, 2025.
- [13] J. Jing, Y. Qin, X. Zhu, H. Shan, and P. Peng, “Identification and prediction of casing collar signal based on cnn-lstm,” *Arabian Journal for Science and Engineering*, pp. 1–15, 2024.
- [14] Z. E. Ross, M.-A. Meier, E. Hauksson, and T. H. Heaton, “Generalized seismic phase detection with deep learning,” *Bulletin of the Seismological Society of America*, vol. 108, no. 5A, pp. 2894–2901, 2018.
- [15] A. Le Guennec, S. Malinowski, and R. Tavenard, “Data augmentation for time series classification using convolutional neural networks,” in *ECML/PKDD workshop on advanced analytics and learning on temporal data*, 2016.
- [16] Q. Wen, T. Zhou, C. Zhang, W. Chen, Z. Ma, J. Yan, and L. Sun, “Transformers in time series: A survey,” *arXiv preprint arXiv:2202.07125*, 2022.
- [17] M. Raissi, P. Perdikaris, and G. E. Karniadakis, “Physics-informed neural networks: A deep learning framework for solving forward and inverse problems involving nonlinear partial differential equations,” *Journal of Computational physics*, vol. 378, pp. 686–707, 2019.
- [18] K. Noh, D. Pardo, and C. Torres-Verdín, “Deep-learning inversion method for the interpretation of noisy logging-while-drilling resistivity measurements,” *arXiv preprint arXiv:2111.07490*, 2021.
- [19] P. Murugan and S. Durairaj, “Regularization and optimization strategies in deep convolutional neural network,” *arXiv preprint arXiv:1712.04711*, 2017.
- [20] S. Ioffe and C. Szegedy, “Batch normalization: Accelerating deep network training by reducing internal covariate shift,” in *International conference on machine learning*. pmlr, 2015, pp. 448–456.
- [21] S. Santurkar, D. Tsipras, A. Ilyas, and A. Madry, “How does batch normalization help optimization?” *Advances in neural information processing systems*, vol. 31, 2018.
- [22] N. Bjorck, C. P. Gomes, B. Selman, and K. Q. Weinberger, “Understanding batch normalization,” *Advances in neural information processing systems*, vol. 31, 2018.
- [23] M. R. Asif, T. S. Bording, A. S. Barfod, E. Auken, and J. J. Larsen, “Effect of data normalization on neural networks for the forward

modelling of transient electromagnetic data,” in *NSG2020 26th European Meeting of Environmental and Engineering Geophysics*, vol. 2020, no. 1. European Association of Geoscientists & Engineers, 2020, pp. 1–5.

[24] Y. Yang, K. Zha, Y. Chen, H. Wang, and D. Katabi, “Delving into deep imbalanced regression,” in *International conference on machine learning*. PMLR, 2021, pp. 11 842–11 851.

[25] C. Szegedy, V. Vanhoucke, S. Ioffe, J. Shlens, and Z. Wojna, “Rethinking the inception architecture for computer vision,” in *Proceedings of the IEEE conference on computer vision and pattern recognition*, 2016, pp. 2818–2826.

[26] D. Stoller, S. Ewert, and S. Dixon, “Wave-u-net: A multi-scale neural network for end-to-end audio source separation,” *arXiv preprint arXiv:1806.03185*, 2018.

[27] A. Krizhevsky, I. Sutskever, and G. E. Hinton, “Imagenet classification with deep convolutional neural networks,” *Communications of the ACM*, vol. 60, no. 6, pp. 84–90, 2017.

[28] A. Krizhevsky, “One weird trick for parallelizing convolutional neural networks,” *arXiv preprint arXiv:1404.5997*, 2014.

[29] X. Geng, “Label distribution learning,” *IEEE Transactions on Knowledge and Data Engineering*, vol. 28, no. 7, pp. 1734–1748, 2016.

[30] Y. LeCun, L. Bottou, G. B. Orr, and K.-R. Müller, “Efficient backprop,” in *Neural networks: Tricks of the trade*. Springer, 2002, pp. 9–50.